ADVANCED FUNCTIONAL MATERIALS
www.afm-journal.de

Tribotronic Phototransistor for Enhanced Photodetection and Hybrid Energy Harvesting

*Chi Zhang, Zhao Hua Zhang, Xiang Yang, Tao Zhou, Chang Bao Han, and Zhong Lin Wang**

Tribotronics is a new field developed by coupling triboelectricity and semiconductor, which can drive triboelectric-charge-controlled optoelectronic devices by further introducing optoelectronics. In this paper, a tribotronic phototransistor (TPT) is proposed by coupling a field-effect phototransistor and a triboelectric nanogenerator (TENG), in which the contact-induced inner gate voltage by the mobile frictional layer is used for modulating the photodetection characteristics of the TPT. Based on the TPT, alternatively, a coupled energy-harvester (CEH) is fabricated for simultaneously scavenging solar and wind energies, in which the output voltage on the external resistance from the wind driven TENG is used as the gate voltage of the TPT for enhancing the solar energy conversion. As the wind speed increases, the photovoltaic characteristics of the CEH including the short-circuit current, open-circuit voltage, and maximal output power have been greatly enhanced. This work has greatly expanded the functionality of tribotronics in photodetection and energy harvesting, and provided a potential solution for highly efficient harvesting and utilizing multitype energy.

1. Introduction

Optoelectronics is an emerging and quickly developing technology over the past decades, which has great applications in display, illumination, sensor, and energy harvesting.[1,2] With the increasing significance of nanotechnology in semiconductor, nanomaterials exhibit tremendous potential in optoelectronics, such as light-emitting diodes,[3] photodetector,[4] and photocell.[5] However, most of the reported photoelectric devices are still suffering from difficulties of further improving the photoelectric characteristics and lacking of adjustability.

Dr. C. Zhang, Dr. Z. H. Zhang, T. Zhou,
Dr. C. B. Han, Prof. Z. L. Wang
Beijing Institute of Nanoenergy and Nanosystems
Chinese Academy of Sciences
Beijing 100083, China
E-mail: zlwang@gatech.edu
Dr. X. Yang
Institute of Semiconductors
Chinese Academy of Sciences
Beijing 100083, P. R. China
Prof. Z. L. Wang
School of Material Science and Engineering
Georgia Institute of Technology
Atlanta, GA 30332-0245, USA

DOI: 10.1002/adfm.201504919

As a three-way coupling effect among semiconductor, piezoelectricity, and photoexcitation, the piezo-phototronic effect was first proposed in 2010[6] and has demonstrated strain-enhanced light-emitting diodes,[7,8] photodetectors,[9,10] and photocells[11,12] by modulating the charge carrier transport, separation, or recombination through strain-induced piezoelectric polarization charges. Recently, the invention of a triboelectric nanogenerator (TENG) has provided not only sustainable power sources[13–17] and self-powered devices,[18–20] but also proposed triboelectric-charge-controlled devices[21–23] and opened up a new research field of tribotronics.[24,25] Since 2014, various tribotronic devices have been studied using the electrostatic potential created by triboelectrification as a "gate" voltage to tune/control charge carrier transport in the semiconductor.[26–29] By further introducing optoelectronics, the tribotronic light-emitting diode has been developed as an adjustable electroluminescent device,[27] which has prompted the adjustable photoelectric conversion devices to be highly expected for enhancing the photoelectric conversion performance by triboelectrification.

Here in this work, we proposed a tribotronic phototransistor (TPT) by coupling a field-effect phototransistor and a TENG, in which the contact-induced inner gate voltage by the mobile frictional layer is used for modulating the photoelectric characteristics of the TPT. Based on the TPT, a coupled energy-harvester (CEH) as an alternative design is fabricated by coupling the field-effect phototransistor and a wind driven TENG for simultaneously scavenging solar and wind energies, in which the output voltage on the external resistance from the wind driven TENG is used as the gate voltage of the TPT for enhancing the solar energy conversion with the increase of the wind speed. With the adjustability and enhancement by triboelectrification, the TPT has greatly expanded the functionality of tribotronics in photodetection and energy harvesting, and provided a potential solution for highly efficient harvesting and utilizing the multitype energy.

2. Principles and Characteristics

2.1. Structure of the TPT

The structure of the TPT is composed of a back-gate silicon-on-insulator (SOI) field-effect phototransistor and a mobile layer, as schematically illustrated in **Figure 1**a. In the fabrication of

ADVANCED FUNCTIONAL MATERIALS
www.afm-journal.de

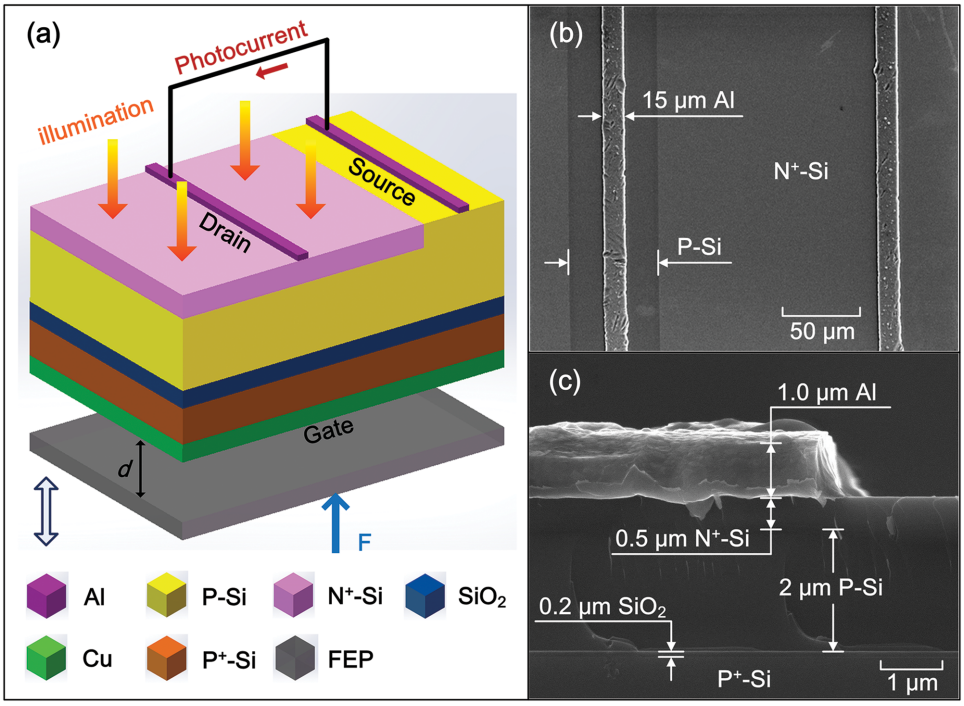

Figure 1. Schematic illustration of the tribotronic phototransistor (TPT). a) Structure of the TPT based on a SOI wafer with pn junction and a mobile layer for vertical contact electrification. b) Partial top view of the TPT. c) Partial cross-sectional view of the TPT.

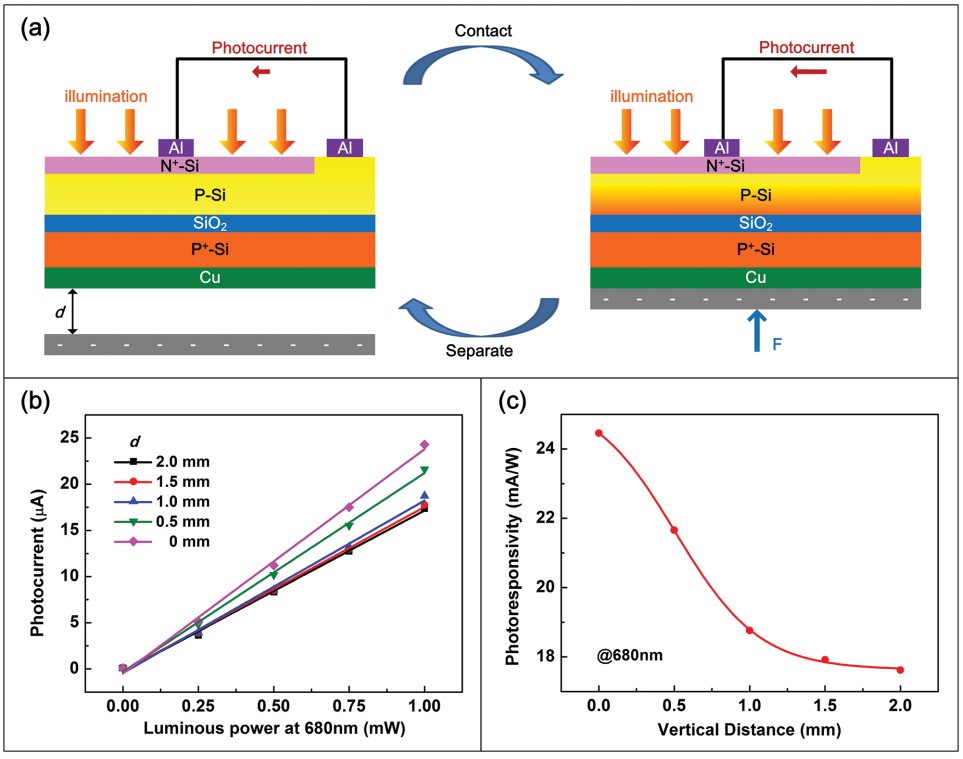

Figure 2. Principle of the TPT for enhancing photodetection characteristics. a) Change of the gate voltage and channel carrier concentration in the TPT when the mobile layer contacts with and separates from the gate electrode to demonstrate the working principle. b) Photoelectric characteristics of the TPT with different vertical distance from 0 to 2.0 mm. c) Photoresponsivity transfer characteristics of the TPT with the illumination at 680 nm.

Adv. Funct. Mater. **2016**,
DOI: 10.1002/adfm.201504919

the TPT device, a heavily doped n-type silicon layer is formed on the partial surface of the p-type conduction channel layer as a pn junction by the phosphorus ion implantation at 80 keV with a dose of 8E15 ions per cm^2, and then rapid thermal annealing at 1050 °C for 1 min. The heavily doped n-type silicon layer is about 0.5 μm deep in the top silicon layer of 2.5 μm thick. Two aluminum electrodes of 1.0 μm thick and 15 μm wide are deposited on the surface of the p-type and n-type silicon layers with Ohmic contacts, serving as the drain and source, respectively. A copper layer is deposited on the bottom of the heavily doped silicon substrate with Ohmic contact, serving as the gate electrode. The buried silicon dioxide layer of 0.2 μm thick between them is used as the gate oxide. Underneath the gate electrode, a mobile fluorinated ethylene propylene (FEP) layer is selected for triboelectrification, which can vertically contact with and separate from the gate electrode by an external force. The scanning electron microscope (SEM) images of the TPT in the partial top view and cross-sectional view are shown in Figure 1b,c, respectively.

According to the photovoltaic effect in pn junction, a photocurrent can be generated in the conduction channel of the field-effect phototransistor by the external illumination. By applying an external voltage as shown in Figure S1a (Supporting Information), Figure S1b (Supporting Information) shows the output characteristics of the pn junction with different illuminous power from 0.25 to 1 mW at 680 nm. The measured results are similar to the classical photodiode behavior and demonstrate the favorable photoelectric properties of the pn junction.

2.2. Principle and Characteristics for Enhanced Photodetection

The working principle of the TPT is based on the coupling effects of the field-effect phototransistor and the TENG in single-electrode mode, which is schematically shown in **Figure 2**a. In the original state, the top surface of the mobile FEP layer has initial negative charges by contact electrification with the gate electrode. The initial positive charges on the gate electrode are neutralized by grounding, and the initial gate voltage is set to zero in this state. As the mobile FEP layer is separated from the gate electrode at a certain distance, it has no effects on the gate voltage of the field-effect phototransistor. With the illumination, the photocurrent is generated and flowed through the conduction channel. When the external force is applied and the mobile FEP layer is vertically contacted with the gate electrode, a negative gate voltage is generated to the phototransistor by the electrostatic induction effect of the negative charges on the FEP layer. An enhancement zone is, thus, formed in the p-type top silicon layer to increase the photocurrent. When the external force is released and the mobile FEP layer is separated from the gate electrode at a certain distance again, the gate voltage turns back to zero and the conduction channel is recovered, which will decrease the photocurrent to the original state. Therefore, by decreasing the gap distance d between the mobile FEP layer and the gate electrode, the conduction channel of the phototransistor can be broadened and the photoelectric characteristics of the TPT can be enhanced by the applied negative triboelectric charges.

The gap distance d of the TPT can be well-controlled by a precise positioning system for the characterization. Figure 2b shows the photoelectric characteristics of the TPT with different vertical distance d from 0 to 2.0 mm, and Figure 2c shows the photoresponsivity transfer characteristics of the TPT with the illumination at 680 nm. The experimental results indicate that the photocurrent has a linear relationship with the illumination and is increased with the decreasing distance, which is in accordance with the working principle in Figure 2a. When the distance decreases from 2.0 to 0 mm, the p-type conduction channel in the top silicon layer is broadened and the photoresponsivity with the illumination at 680 nm is increased from 17.6 to 24.5 mA W^{-1}. The experimental results are compared with the characteristics of the field-effect phototransistor by applying an external gate voltage, which is schematically illustrated in Figure S2a (Supporting Information). Figure S2b (Supporting

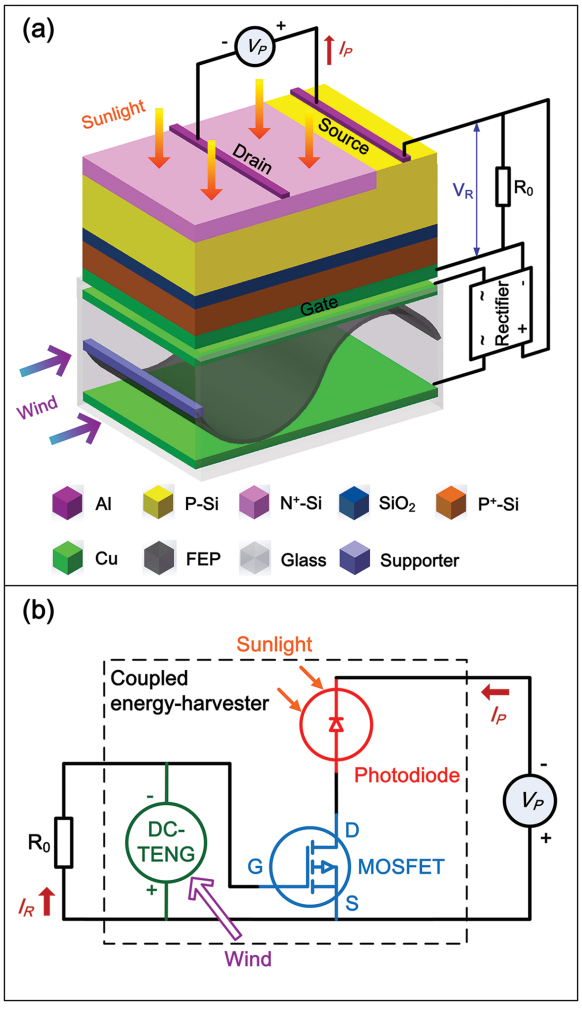

Figure 3. Coupled energy-harvester (CEH) as an alternative design of the TPT for simultaneously scavenging wind and solar energies. a) Schematic illustration of the CEH. The output voltage on the external resistance from the wind driven TENG is used as the gate voltage of the TPT for enhancing the solar energy conversion. b) Equivalent circuit diagram of the CEH, which can be described as the integration of a photodiode, a metal oxide semiconductor field effect transistor (MOSFET) and a direct-current TENG.

Information) shows the photoelectric characteristics at different gate voltage, and Figure S2c (Supporting Information) shows the photoresponsivity is increased from 17.6 to 26.8 mA W^{-1} with the gate voltage decreases from 0 to −8 V. The comparison results show the similar characteristics and indicate that the applied external force to the TPT has the same effects of applying negative gate voltage to the phototransistor, which has successfully enhanced the photoelectric characteristics of the TPT. Therefore, based on the field-effect phototransistor and the TENG, the TPT has been realized as a new tribo-phototronic device to first demonstrate the triboelectric-charge-enhanced photoelectric conversion.

2.3. Structure and Principle of the TPT as a CEH

Besides the photodetection, the TPT can be used for scavenging solar energy based on the photovoltaic effect, and the triboelectric charges used for modulating the TPT can be also generated from the ambient energy. As an alternative design of the TPT, a CEH is fabricated by integrating the field-effect phototransistor and a wind driven TENG for simultaneously scavenging solar and wind energies, which is schematically illustrated in **Figure 3**a. The wind driven TENG consists of two copper foils in top and bottom of a cuboid acrylic tube, respectively, and a FEP film in the middle of them,[30,31] which is in dimensions of 3.0 × 3.0 × 5.0 cm^3. One side of the FEP film is on an acrylic sheet at the middle of the end surface of the tube, while the other side is freestanding. The wind driven vibration of the FEP film can induce the periodical contact with and separation from the top and bottom copper electrodes, resulting in a direct voltage output across an external load resistor through a rectifier, which is applied on the phototransistor as the negative gate voltage. The equivalent circuit diagram of the CEH can be described as the integration of a photodiode, a metal oxide semiconductor field-effect transistor (MOSFET), and a direct-current (DC) TENG, as shown in Figure 3b. The photodiode connects in series with the MOSFET and collects solar energy

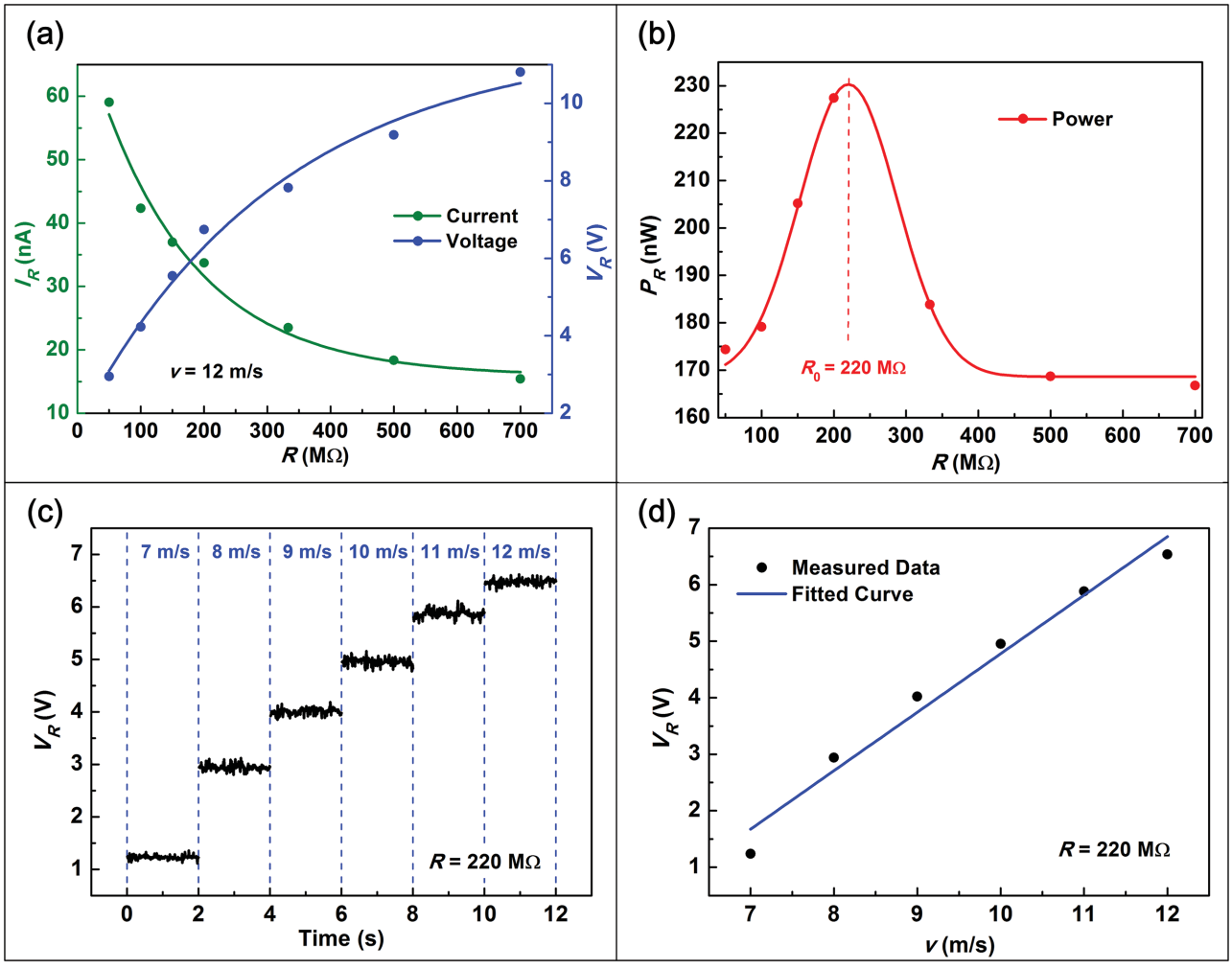

Figure 4. Characteristics of the wind energy harvesting. a) The relationship between the output current/voltage and the load resistance at a wind speed of 12 m s^{-1}. b) The relationship between the output power and the load resistance. The maximum power is received when the external resistance is 220 MΩ. c) The measured output voltage across the load resistance of 220 MΩ with different wind speeds from 7 to 12 m s^{-1}. d) The summarized relationship between the output voltage and the wind speed.

Adv. Funct. Mater. **2016**,
DOI: 10.1002/adfm.201504919

as a power source, while the DC-TENG collects wind energy and provides an electric power to the external load resistor, in which the output voltage is also used for enhancing the solar energy conversion.

2.4. Characteristics for Hybrid Energy Harvesting

The CEH is located in a flowing air generated by a wind simulator with accurate speeds. **Figure 4**a shows the resistance dependence of both output current and voltage, from 50 to 700 MΩ at a wind speed of 12 m s^{-1}, and Figure 4b plots the output power as a function of the resistance. The output current decreases with the increasing resistance while the output voltage shows the reverse trend. The maximum output power of 231 nW is received when the load resistance is 220 MΩ. The measured output voltage across the load resistance of 220 MΩ with different wind speeds from 7 to 12 m s^{-1} is demonstrated in Figure 4c, and the summarized relationship between the output voltage and the wind speed is shown in Figure 4d. It can be clearly seen that the output voltage is nearly constant at each fixed wind speed, and dramatically increases with the increasing wind speed. A linear relationship between them can be obtained by fitting the data with the sensitivity of about 1.04 V $(m\ s^{-1})^{-1}$, which indicates that the applied gate voltage for modulating the phototransistor can be stably and linearly generated by the wind-induced triboelectrification.

The CEH is irradiated using a solar simulator to accurately simulate sunlight intensity. The measured I_P–V_P characteristics of the CEH with different sunlight intensity without wind are presented in **Figure 5**a. It is clearly seen that the photovoltaic characteristics including the short-circuit current and open-circuit voltage are increased with the increasing sunlight intensity. The measured I_P–V_P characteristics of the CEH with different wind speed from 7 to 11 m s^{-1} at the sunlight intensity of 2 mW cm^{-2} are shown in Figure 5b, and the dependence of the short-circuit current, open-circuit voltage, and maximal output power on the wind speed at the sunlight intensity of 2 mW cm^{-2} are

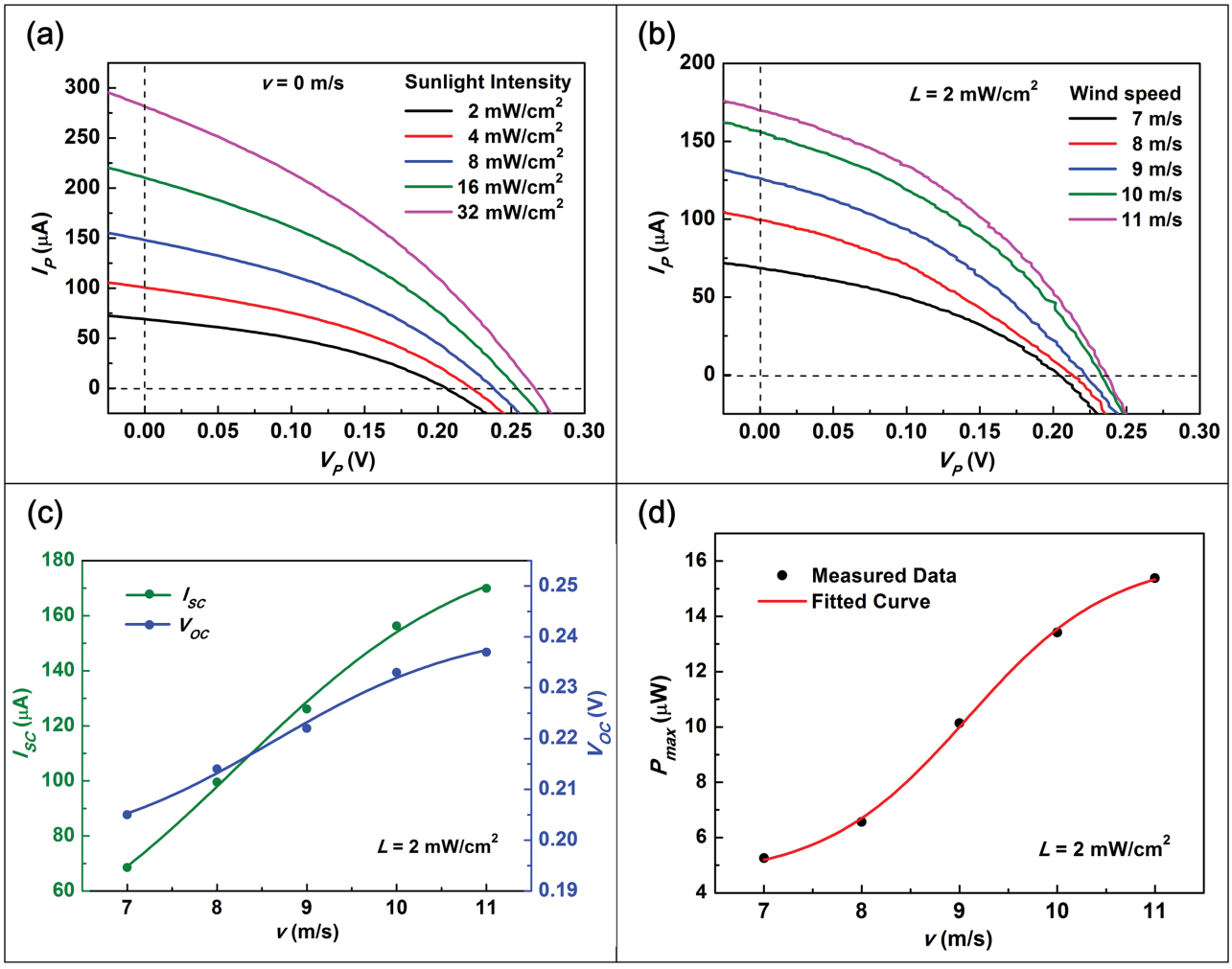

Figure 5. Characteristics of the solar energy harvesting coupled by wind. a) I_P–V_P characteristics with different sunlight intensity without wind. b) I_P–V_P characteristics with different wind speed from 7 to 11 m s^{-1} at the sunlight intensity of 2 mW cm^{-2}. c,d) Dependence of the c) short-circuit current, open-circuit voltage, and d) maximal output power on the wind speed at the sunlight intensity of 2 mW cm^{-2}.

presented in Figure 5c,d, respectively. The experimental results indicate that the photovoltaic performance of the CEH is nearly steady at each different wind speed and significantly increases with the increasing wind speed. It can be found that the short-circuit current increased from 68.6 to 170.7 μA and the open-circuit voltage increased from 0.21 to 0.24 V, about 149% and 14.3% incensements, respectively. The calculated maximal output power is also enhanced from 5.3 to 15.4 μW with 191% enhancement. At the different sunlight intensities of 4 and 8 mW cm^{-2}, Figure S3 (Supporting Information) has also shown the dependence of the photovoltaic characteristics on the wind speed, respectively, in which the CEH has similar characteristics and the performances can also be greatly enhanced as the wind speed increases.

Therefore, the CEH has been realized for simultaneously harvesting solar and wind energies and the photovoltaic performance can be enhanced by wind, different from the conventional photocell for harvesting only solar energy. This new tribo-phototronic device has provided a potential solution to improve the photovoltaic performance of the photocell, for that the solar energy is often along with the wind energy in natural environment. It is worth noting that the increased solar energy harvesting power by the wind driven TENG is far greater than the maximal output power of itself, which is only 231 nW at the wind speed of 12 m s^{-1}. The CEH has established an effective coupling mechanism between different energy transducers other than the independent operations with each other, which has demonstrated favorable effects on hybrid energy harvesting and conversion.

3. Conclusion

In summary, by coupling a field-effect phototransistor and a TENG in single-electrode mode, a TPT has been proposed, in which the contact-induced inner gate voltage by the mobile frictional layer is used for modulating the photodetection characteristics of the phototransistor. On basis of the TPT, a CEH as an alternative design has been fabricated by coupling the field-effect phototransistor and a wind driven TENG for simultaneously scavenging solar and wind energies, in which the output voltage on the external resistance from the wind driven TENG is used as the inner gate voltage of the TPT for enhancing the solar energy conversion. As the wind speed increases, the photovoltaic characteristics of the CEH including the short-circuit current, open-circuit voltage, and maximal output power have been greatly enhanced. Different from the conventional photocell for harvesting only solar energy, the CEH can harvest the wind energy simultaneously for enhancing the photovoltaic performances. As a new tribo-phototronic device, the TPT has not only demonstrated the triboelectric-charge-enhanced photodetection, but also established an effective coupling mechanism between different energy transducers and demonstrated the triboelectric-charge-enhanced hybrid energy harvesting. This work has greatly expanded the functionality of tribotronics in photodetection and energy harvesting, and provided a potential solution for highly efficient harvesting and utilizing the multitype energy.

Supporting Information

Supporting Information is available from the Wiley Online Library or from the author.

Acknowledgements

C.Z. and Z.H.Z. contributed equally to this work. The project was supported by the National Natural Science Foundation of China (Grant Nos. 51475099, 51432005, and 5151101243), the "thousands talents" program for the pioneer researcher and his innovation team, China, and the Youth Innovation Promotion Association, CAS. The authors also thank Chaoying Zhang for her assistance in the SEM images analysis and Fengben Xi for his assistance in the wind driven TENG fabrication.

Received: November 16, 2015
Revised: December 24, 2015
Published online:

[1] Y. Li, F. Qian, J. Xiang, C. M. Lieber, *Mater. Today* **2006**, *9*, 18.
[2] F. Bonaccorso, Z. Sun, T. Hasan, A. C. Ferrari, *Nat. Photonics* **2010**, *4*, 611.
[3] J. Bao, M. A. Zimmler, F. Capasso, X. Wang, Z. F. Ren, *Nano Lett.* **2006**, *6*, 1719.
[4] F. Xia, T. Mueller, Y. Lin, A. V. Garcia1, P. Avouris, *Nat. Nanotechnol.* **2009**, *4*, 839.
[5] S. H. Ko, D. Lee, H. W. Kang, K. H. Nam, J. Y. Yeo, S. J. Hong, C. P. Grigoropoulos, H. J. Sung, *Nano Lett.* **2011**, *11*, 666.
[6] Z. L. Wang, *J. Phys. Chem. Lett.* **2010**, *1*, 1388.
[7] Y. Liu, S. Niu, Q. Yang, B. D. Klein, Y. S. Zhou, Z. L. Wang, *Adv. Mater.* **2014**, *26*, 7209.
[8] Q. Yang, Y. Liu, C. F. Pan, J. Chen, X. N. Wen, Z. L. Wang, *Nano Lett.* **2013**, *13*, 607.
[9] Q. Yang, X. Guo, W. H. Wang, Y. Zhang, S. Xu, D. H. Lien, Z. L. Wang, *ACS Nano* **2010**, *4*, 6285.
[10] F. Zhang, S. Niu, W. Guo, G. Zhu, Y. Liu, X. L. Zhang, Z. L. Wang, *ACS Nano* **2013**, *7*, 4537.
[11] X. N. Wen, W. Z. Wu, Z. L. Wang, *Nano Energy* **2013**, *2*, 1093.
[12] Z. Wang, R. Yu, X. Wen, Y. Liu, C. Pan, W. Wu, Z. L. Wang, *ACS Nano* **2014**, *8*, 12866.
[13] C. Zhang, W. Tang, C. B. Han, F. R. Fan, Z. L. Wang, *Adv. Mater.* **2014**, *26*, 3580.
[14] C. Zhang, T. Zhou, W. Tang, C. B. Han, L. M. Zhang, Z. L. Wang, *Adv. Energy Mater.* **2014**, *4*, 1301798.
[15] C. B. Han, C. Zhang, W. Tang, X. H. Li, Z. L. Wang, *Nano Res.* **2015**, *8*, 722.
[16] Q. Liang, X. Yan, X. Liao, S. Cao, X. Zheng, H. Si, S. Lu, Y. Zhang, *Nano Energy* **2015**, *16*, 329.
[17] Q. Liang, X. Yan, Y. Gu, K. Zhang, M. Liang, S. Lu, X. Zheng, Y. Zhang, *Sci. Rep.* **2015**, *5*, 9080.
[18] C. B. Han, C. Zhang, X. H. Li, L. M. Zhang, T. Zhou, W. G. Hu, Z. L. Wang, *Nano Energy* **2014**, *9*, 325.
[19] Y. K. Pang, X. H. Li, M. X. Chen, C. B. Han, C. Zhang, Z. L. Wang, *ACS Appl. Mater. Inter.* **2015**, *7*, 19076.
[20] L. M. Zhang, F. Xue, W. M. Du, C. B. Han, C. Zhang, Z. L. Wang, *Nano Res.* **2014**, *7*, 1215.
[21] C. Zhang, W. Tang, Y. K. Pang, C. B. Han, Z. L. Wang, *Adv. Mater.* **2015**, *27*, 719.
[22] C. B. Han, C. Zhang, J. J. Tian, X. H. Li, L. M. Zhang, Z. Li, Z. L. Wang, *Nano Res.* **2014**, *8*, 219.
[23] X. Y. Chen, M. Iwamoto, Z. Shi, L. M. Zhang, Z. L. Wang, *Adv. Funct. Mater.* **2014**, *25*, 739.

[24] C. Zhang, W. Tang, L. M. Zhang, C. B. Han, Z. L. Wang, *ACS Nano* **2014**, *8*, 8702.
[25] Y. Liu, S. Niu, Z. L. Wang, *Adv. Electron. Mater.* **2015**, *1*, 1500124.
[26] C. Zhang, L. M. Zhang, W. Tang, C. B. Han, Z. L. Wang, *Adv. Mater.* **2015**, *27*, 3533.
[27] C. Zhang, J. Li, C. B. Han, L. M. Zhang, X. Y. Chen, L. D. Wang, G. F. Dong, Z. L. Wang, *Adv. Funct. Mater.* **2015**, *25*, 5625.
[28] J. Li, C. Zhang, L. Duan, L. M. Zhang, L. D. Wang, G. F. Dong, Z. L. Wang, *Adv. Mater.* **2016**, *28*, 106.
[29] F. Xue, L. Chen, L. Wang, Y Pang, J. Chen, C. Zhang, Z. L. Wang, *Adv. Funct. Mater.* **2016**, unpublished.
[30] Y. Yang, G. Zhu, H. Zhang, J. Chen, X. Zhong, Z. H. Lin, Y. Su, P. Bai, X. Wen, Z. L. Wang, *ACS Nano* **2013**, *7*, 9461.
[31] S. Wang, X. Mu, Y. Yang, C. Sun, A. Y. Gu, Z. L. Wang, *Adv. Mater.* **2015**, *27*, 240.